Journal of Nanoparticle Research

A block elimination algorithm for multiple scattering of multilayered concentric nanoparticle aggregates

--Manuscript Draft--

Manuscript Number:	NANO-D-22-01957
Full Title:	A block elimination algorithm for multiple scattering of multilayered concentric nanoparticle aggregates
Article Type:	Original research
Keywords:	Multiple scattering · Block elimination · Nanoparticle aggregates
Corresponding Author:	Ben Q Li, Ph.D. University of Michigan Dearborn, MI UNITED STATES
Corresponding Author Secondary Information:	
Corresponding Author's Institution:	University of Michigan
Corresponding Author's Secondary Institution:	
First Author:	Rongheng Li
First Author Secondary Information:	
Order of Authors:	Rongheng Li
	Ben Q Li, Ph.D.
Order of Authors Secondary Information:	
Funding Information:	
Abstract:	An efficient block elimination method is developed for the calculation of the multi-scattering of electromagnetic waves by multilayered concentric nanoparticle aggregates. Instead of applying the LU decomposition or Gaussian elimination method as commonly used for the solution of global translation matrix, the present method partitions the matrix into blocks based on the number of particles in the aggregate and performs the elimination process blocks by blocks. A key advantage of this method is that the pivot block needs to be inverted only once, thereby reducing the computational time. This, in combination with a progressive algorithm for a multilayer concentric particle, provides a very efficient numerical procedure for the solution of scattering coefficients for a multilayered concentric nanoparticle cluster. Moreover, the computational efficiency is further improved by parallelization of the block-by-block elimination method. The algorithm only requires updating a portion of the matrix during each elimination stage. Numerical testing shows that the computational time is reduced considerably with the proposed parallel block-by-block elimination method. Computed cases are presented, illustrating that the proposed algorithm is effective for the design of multilayered nanoparticle aggregates with various optical phenomena, including maximum forward or backward scattering features.
Suggested Reviewers:	Wen Yang Cold and Arid Regions Environmental and Engineering Research Institute: Northwest Institute of Eco-Environment and Resources ywen@ns.lzb.ac.cn
	Yu-lin Xu The University of Texas at El Paso yxu5@utep.edu
Additional Information:	
Question	**Response**

Scientific Justification (Available to Reviewers)	Dear Editor and Reviewers: Enclosed please find the paper titled, “A block elimination algorithm for multiple scattering of multilayered concentric nanoparticle aggregates”, which is to be submitted to the Journal of Nanoparticle Research. The paper presents an efficient block elimination approach to calculate the electromagnetic scattering of nanoparticle aggregates containing multilayered nanoshells. Unlike the well-known algorithms reported in other works, this proposed method partitions the matrix into blocks based on the number of particles in the aggregate and performs the elimination process blocks by blocks. Moreover, parallelization of the eliminations further improves the calculation efficiency. In addition, the pivot block needs to be inverted only once, thereby reducing the computational time. Combined with a progressive algorithm for multilayered concentric nanoshells, this approach provides a very efficient numerical methodology for the solution of multiple scattering of a multilayered nanoparticle aggregate. The case study demonstrates that the presented methodology can assist the design of multilayered core/shell nanoparticle clusters with distinct optical phenomena, including maximum forward or backward scattering features. My co-authors and I are delighted if you could consider the paper for publication in the Journal of Nanoparticle Research. Sincerely, Ben Q. Li, Ph.D., Fellow of ASME Professor and Chair

A block elimination algorithm for multiple scattering of multilayered concentric nanoparticle aggregates

RONGHENG LI AND BEN Q. LI*

Department of Mechanical Engineering, University of Michigan, Dearborn, MI 48128, United States

**benqli@umich.edu*

Abstract: An efficient block elimination method is developed for the calculation of the multi-scattering of electromagnetic waves by multilayered concentric nanoparticle aggregates. Instead of applying the LU decomposition or Gaussian elimination method as commonly used for the solution of global translation matrix, the present method partitions the matrix into blocks based on the number of particles in the aggregate and performs the elimination process blocks by blocks. A key advantage of this method is that the pivot block needs to be inverted only once, thereby reducing the computational time. This, in combination with a progressive algorithm for a multilayer concentric particle, provides a very efficient numerical procedure for the solution of scattering coefficients for a multilayered concentric nanoparticle cluster. Moreover, the computational efficiency is further improved by parallelization of the block-by-block elimination method. The algorithm only requires updating a portion of the matrix during each elimination stage. Numerical testing shows that the computational time is reduced considerably with the proposed parallel block-by-block elimination method. Computed cases are presented, illustrating that the proposed algorithm is effective for the design of multilayered nanoparticle aggregates with various optical phenomena, including maximum forward or backward scattering features.

Keywords

Multiple scattering · Block elimination · Nanoparticle aggregates

1. Introduction

Plasmonic nanoparticles comprise noble metals and high refractive index dielectrics possess extraordinary optical properties, i.e., super scattering ability, high absorption efficiency, and unique directional scattering features. Such excellent optical properties enable them attractive for various applications, including photocatalysis[1–5], photovoltaics[6–9], hyperthermia therapy[10–14], biosensing[15–19], and optical communication[20–23]. The scattering and absorption responses of a nanoparticle are analytically described by the well-known Mie theory[24]. By engineering the shape, dimension, and material composition of the nanoparticle, the desired optical behavior can be obtained for a specific frequency[25–27]. However, the optical tunability is quite limited for solid nanospheres. Nanoshells with multilayered core-shell structures are introduced to provide more flexibility in tuning the peak wavelength, and hence the plasmonic resonance scattering efficiency and absorption efficiency[28, 29]. Moreover, nanoparticle aggregates further extend this capability to create more interesting optical characteristics by exploring certain electromagnetic interactions among particles[30, 31]. In such cases, the arrangement and gap distance between particles provide extra freedoms of tunability.

The design of multiparticle systems for engineering applications relies on the ability to compute the optical responses of the multilayered particle aggregates. Considerable progress has been made in recently in solving the scattering problems of various configurations, i.e., individual multilayered nanoshells[32, 33], multiple solid particles[34–36], and multiple

multilayered core-shell spherical particles[37–39]. One major step in the multiple scattering calculations is translating the scattered field of all particles into predefined coordinates, which is usually the center of a specific particle. By applying the boundary conditions at the outer surface of every particle, a system of equations is formed with the scattering coefficients to be solved. The matrix represents the system equations as the size of $4\times N_{\max}\times NT$ by $4\times N_{\max}\times NT$, where $N_{\max}$ and NT are the highest order of modes needed for the specific case and the number of particles, respectively. As recent research focuses on wave scattering by large-scale particle clusters, the size of the matrix becomes extremely huge. For instance, a recent work[40] reported a calculation of the scattering by an aggregate comprising about 10^4 particles, where a huge system of equations has to be solved. This can result in an exhaustive task in the computation.

To obtain the scattering coefficients efficiently, the matrix that represents the system of equations is manipulated in various approaches. The first method is the direct inversion of the matrix[41], which is straightforward but extremely computationally demanding. Sout *et al.* presented an iterative scheme, where all the fields are expanded from each particle's origin[42]. The matrix representing the linear system of one particle problem is built up first. Afterward, the matrix is extended by adding particles incrementally. In the end, the linear system for the entire particle aggregates is achieved. Distinct from Sout's algorithm, Mackowski *et al.* construct the scattering matrix with all the fields expanded in a common origin[34, 35, 43]. The averaged scattering and absorption coefficients for the multiple-sphere system are calculated efficiently. The above approaches are implemented in numerical programs, including CELES[44], FASTMM[45], SMUTHI[40], QPMS[46], and TERMS[47].

In this paper, an efficient computational methodology is presented for the multiple scattering problem of a multilayered nanoshell aggregate. A block elimination algorithm is proposed to solve the global translation matrix resulting from satisfying boundary conditions at the surface of each particle in an aggregate. This approach reduces the computational burden in two aspects. First, operations for only a portion of blocks are performed in the elimination process, which is distinct from the Gaussian elimination. Second, instead of inverting the pivot block in the operation for every block, it is only computed once and shared for all blocks. Moreover, the computation efficiency is further enhanced by paralleling the block elimination of individual block rows. Combined with the progressive algorithm for a single multilayered nanoshell, this method provides an efficient computational procedure for the study of multiscatting phenomena associated with multilayered nanoshell clusters. Computed results show the computational efficiency enhancement of the proposed approach in comparison with the commonly used LU decomposition method. The approach has been applied in the study of nanoparticle clusters for unique scattering properties. Illustrative study cases with forward or backward scattering features are given.

2. Mathematical analysis

The multiple multilayered core/shell particle configuration under consideration is displayed in Fig. 1. The income electromagnetic wave travels along the $\mathbf{k}$ direction, with the time dependence being $\mathrm{e}^{-i\omega t}$. The optical responses of the particle aggregates are described by the wave form of Maxwell equations,

$$\nabla^2\mathbf{E}+k^2\mathbf{E}=\mathbf{0},\nabla\cdot\mathbf{E}=0,\mathbf{H}=-(\frac{i}{\mu_0\omega})\nabla\times\mathbf{E} \tag{1}$$

where $\mathbf{E}$ and $\mathbf{H}$ are the electric and magnetic fields. $k=\sqrt{\omega m/c}$ with m, c, μ_0 are the refractive index, the speed of light, and the magnetic permeability, respectively.

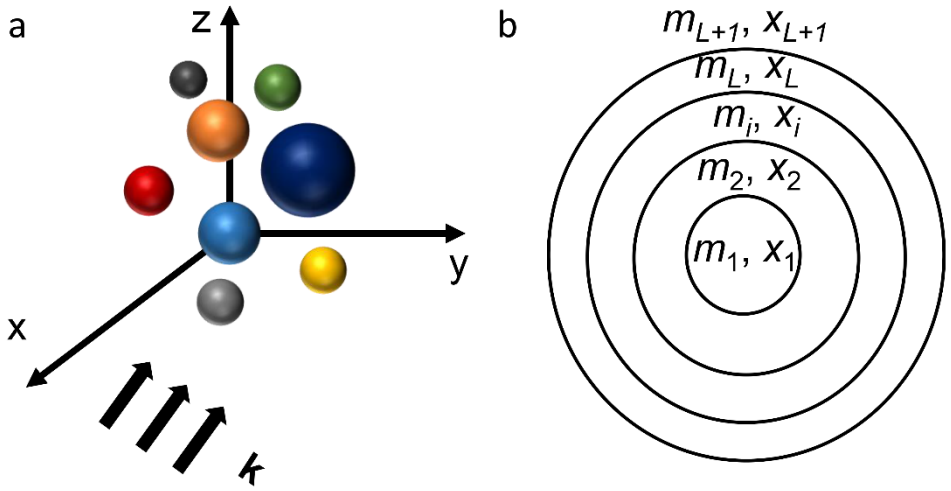

Fig.1. The configuration of the multiple multilayered particles.

To obtain the analytical solution of the wave equations, the scattering coefficients of each particle need to be calculated first. It starts with expanding the electric and magnetic fields in spherical coordinates. For any two adjacent layers, denoted as l and l+1 below, the fields are expressed as

$$\mathbf{E}_l = \sum_{n=1}^{\infty}\sum_{m=-n}^{n} E_n \left(c_{mn}^l \mathbf{M}_{mn,l}^{(1)} + d_{mn}^l \mathbf{N}_{mn,l}^{(1)} + b_{mn}^l \mathbf{M}_{mn,l}^{(3)} + a_{mn}^l \mathbf{N}_{mn,l}^{(3)} \right) \tag{2}$$

$$\mathbf{H}_l = -\frac{im_l}{\omega\mu} \sum_{n=1}^{\infty}\sum_{m=-n}^{n} E_n \left(d_{mn}^l \mathbf{M}_{mn,l}^{(1)} + c_{mn}^l \mathbf{N}_{mn,l}^{(1)} + a_{mn}^l \mathbf{M}_{mn,l}^{(3)} + b_{mn}^l \mathbf{N}_{mn,l}^{(3)} \right) \tag{3}$$

$$\mathbf{E}_{l+1} = \sum_{n=1}^{\infty}\sum_{m=-n}^{n} E_n \left(c_{mn}^{l+1} \mathbf{M}_{mn,l+1}^{(1)} + d_{mn}^{l+1} \mathbf{N}_{mn,l+1}^{(1)} + b_{mn}^{l+1} \mathbf{M}_{mn,l+1}^{(3)} + a_{mn}^{l+1} \mathbf{N}_{mn,l+1}^{(3)} \right) \tag{4}$$

$$\mathbf{H}_{l+1} = -\frac{im_{l+1}}{\omega\mu} \sum_{n=1}^{\infty}\sum_{m=-n}^{n} E_n \left(d_{mn}^{l+1} \mathbf{M}_{mn,l+1}^{(1)} + c_{mn}^{l+1} \mathbf{N}_{mn,l+1}^{(1)} + a_{mn}^{l+1} \mathbf{M}_{mn,l+1}^{(3)} + b_{mn}^{l+1} \mathbf{N}_{mn,l+1}^{(3)} \right) \tag{5}$$

where $E_n = i^n E_0 \left(2n+1\right)/n\left(n+1\right)$. a_{mn} , b_{mn} , c_{mn} , and d_{mn} are the scattering coefficients for the specific layer. $\mathbf{M}_{mn}^{(q)}$ and $\mathbf{N}_{mn}^{(q)}$ are the vector wave functions as

$$\mathbf{M}_{mn}^{(q)} = \frac{im}{\sin\theta} z_n^{(q)}(kr) P_n^m(\cos\theta) e^{im\varphi} \mathbf{e}_\theta - z_n^{(q)}(kr) \frac{\partial P_n^m(\cos\theta)}{\partial\theta} e^{im\varphi} \mathbf{e}_\varphi \tag{6}$$

$$\begin{aligned} \mathbf{N}_{mn}^{(q)} = {} & \frac{1}{kr} z_n^{(q)}(kr) n(n+1) P_n^m(\cos\theta) e^{im\varphi} \mathbf{e}_r + \frac{1}{kr} \frac{\partial\left[rz_n^{(q)}(kr) \right]}{\partial r} \frac{\partial P_n^m(\cos\theta)}{\partial\theta} e^{im\varphi} \mathbf{e}_\theta \\ & + \frac{im}{kr\sin\theta} \frac{\partial\left[rz_n^{(q)}(kr) \right]}{\partial r} P_n^m(\cos\theta) e^{im\varphi} \mathbf{e}_\varphi \end{aligned} \tag{7}$$

where $P_n^m\left(\cos\theta\right)$ are the associated Legendre polynomials. q has values of 1, 2, and 3, representing the spherical Bessel function of the first kind, the second kind, and the spherical Hankel function of the first kind, respectively.

By matching the continuity condition of the tangential fields of layers l and l+1,

$$\left(\mathbf{E}_{l+1}-\mathbf{E}_{l}\right)\times e_r=\mathbf{0} \tag{8}$$

$$\left(\mathbf{H}_{l+1}-\mathbf{H}_{l}\right)\times e_r=\mathbf{0} \tag{9}$$

four equations are obtained as[48]

$$d_{mn}^{l+1}m_l\psi_n^{'}(m_{l+1}x_l)+a_{mn}^{l+1}m_l\xi_n^{'}(m_{l+1}x_l)=d_{mn}^{l}m_{l+1}\psi_n^{'}(m_lx_l)+a_{mn}^{l}m_{l+1}\xi_n^{'}(m_lx_l) \tag{10}$$

$$c_{mn}^{l+1}m_l\psi_n(m_{l+1}x_l)+b_{mn}^{l+1}m_l\xi_n(m_{l+1}x_l)=c_{mn}^{l}m_{l+1}\psi_n(m_lx_l)+b_{mn}^{l}m_{l+1}\xi_n(m_lx_l) \tag{11}$$

$$c_{mn}^{l+1}\psi_n^{'}(m_{l+1}x_l)+b_{mn}^{l+1}\xi_n^{'}(m_{l+1}x_l)=c_{mn}^{l}\psi_n^{'}(m_lx_l)+b_{mn}^{l}\xi_n^{'}(m_lx_l) \tag{12}$$

$$d_{mn}^{l+1}\psi_n(m_{l+1}x_l)+a_{mn}^{l+1}\xi_n(m_{l+1}x_l)=d_{mn}^{l}\psi_n(m_lx_l)+a_{mn}^{l}\xi_n(m_lx_l) \tag{13}$$

where $\psi_n(\rho)$ and $\xi_n(\rho)$ are the Riccati-Bessel functions. The above system equations can be expressed in matrix form as follows,

$$\left[M\right]_l\begin{bmatrix}a_{mn}^{l+1}\\ b_{mn}^{l+1}\\ c_{mn}^{l+1}\\ d_{mn}^{l+1}\end{bmatrix}-\left[N\right]_l\begin{bmatrix}a_{mn}^{l}\\ b_{mn}^{l}\\ c_{mn}^{l}\\ d_{mn}^{l}\end{bmatrix}=0 \tag{14}$$

with

$$\left[M\right]_l=\begin{bmatrix}\xi_n^{'}(m_{l+1}x_l)m_l & 0 & 0 & \psi_n^{'}(m_{l+1}x_l)m_l\\ 0 & \xi_n(m_{l+1}x_l)m_l & \psi_n(m_{l+1}x_l)m_l & 0\\ 0 & \xi_n^{'}(m_{l+1}x_l) & \psi_n^{'}(m_{l+1}x_l) & 0\\ \xi_n(m_{l+1}x_l) & 0 & 0 & \psi_n(m_{l+1}x_l)\end{bmatrix} \tag{15}$$

$$\left[N\right]_l=\begin{bmatrix}\xi_n^{'}(m_lx_l)m_{l+1} & 0 & 0 & \psi_n^{'}(m_lx_l)m_{l+1}\\ 0 & \xi_n(m_lx_l)m_{l+1} & \psi_n(m_lx_l)m_{l+1} & 0\\ 0 & \xi_n^{'}(m_lx_l) & \psi_n^{'}(m_lx_l) & 0\\ \xi_n(m_lx_l) & 0 & 0 & \psi_n(m_lx_l)\end{bmatrix} \tag{16}$$

With simple manipulations of Eqs. (14-16), the following expression is obtained,

$$\begin{bmatrix}a_{mn}^{l+1}\\ b_{mn}^{l+1}\\ c_{mn}^{l+1}\\ d_{mn}^{l+1}\end{bmatrix}=\left[P\right]_l\begin{bmatrix}a_{mn}^{l}\\ b_{mn}^{l}\\ c_{mn}^{l}\\ d_{mn}^{l}\end{bmatrix} \tag{17}$$

where

$$\left[P\right]_l=\left[M\right]_l^{-1}\left[N\right]_l=\begin{bmatrix}p_{11}^{l} & 0 & 0 & p_{14}^{l}\\ 0 & p_{22}^{l} & p_{23}^{l} & 0\\ 0 & p_{32}^{l} & p_{33}^{l} & 0\\ p_{41}^{l} & 0 & 0 & p_{44}^{l}\end{bmatrix} \tag{18}$$

and

$$p_{11}^{l}=\frac{m_{l+1}\xi_n^{'}(m_l x_l)\psi_n(m_{l+1}x_l)-m_l\xi_n(m_l x_l)\psi_n^{'}(m_{l+1}x_l)}{m_l\xi_n^{'}(m_{l+1}x_l)\psi_n(m_{l+1}x_l)-m_l\xi_n(m_{l+1}x_l)\psi_n^{'}(m_{l+1}x_l)} \tag{19}$$

$$p_{14}^{l}=\frac{m_{l+1}\psi_n^{'}(m_l x_l)\psi_n(m_{l+1}x_l)-m_l\psi_n(m_l x_l)\psi_n^{'}(m_{l+1}x_l)}{m_l\xi_n^{'}(m_{l+1}x_l)\psi_n(m_{l+1}x_l)-m_l\xi_n(m_{l+1}x_l)\psi_n^{'}(m_{l+1}x_l)} \tag{20}$$

$$p_{22}^{l}=\frac{m_l\xi_n^{'}(m_l x_l)\psi_n(m_{l+1}x_l)-m_{l+1}\xi_n(m_l x_l)\psi_n^{'}(m_{l+1}x_l)}{m_l\xi_n^{'}(m_{l+1}x_l)\psi_n(m_{l+1}x_l)-m_l\xi_n(m_{l+1}x_l)\psi_n^{'}(m_{l+1}x_l)} \tag{21}$$

$$p_{23}^{l}=\frac{m_l\psi_n^{'}(m_l x_l)\psi_n(m_{l+1}x_l)-m_{l+1}\psi_n(m_l x_l)\psi_n^{'}(m_{l+1}x_l)}{m_l\xi_n^{'}(m_{l+1}x_l)\psi_n(m_{l+1}x_l)-m_l\xi_n(m_{l+1}x_l)\psi_n^{'}(m_{l+1}x_l)} \tag{22}$$

$$p_{32}^{l}=\frac{m_{l+1}\xi_n^{'}(m_{l+1}x_l)\xi_n(m_l x_l)-m_l\xi_n(m_{l+1}x_l)\xi_n^{'}(m_l x_l)}{m_l\xi_n^{'}(m_{l+1}x_l)\psi_n(m_{l+1}x_l)-m_l\xi_n(m_{l+1}x_l)\psi_n^{'}(m_{l+1}x_l)} \tag{23}$$

$$p_{33}^{l}=\frac{m_{l+1}\xi_n^{'}(m_{l+1}x_l)\psi_n(m_l x_l)-m_l\xi_n(m_{l+1}x_l)\psi_n^{'}(m_l x_l)}{m_l\xi_n^{'}(m_{l+1}x_l)\psi_n(m_{l+1}x_l)-m_l\xi_n(m_{l+1}x_l)\psi_n^{'}(m_{l+1}x_l)} \tag{24}$$

$$p_{41}^{l}=\frac{m_l\xi_n^{'}(m_{l+1}x_l)\xi_n(m_l x_l)-m_{l+1}\xi_n(m_{l+1}x_l)\xi_n^{'}(m_l x_l)}{m_l\xi_n^{'}(m_{l+1}x_l)\psi_n(m_{l+1}x_l)-m_l\xi_n(m_{l+1}x_l)\psi_n^{'}(m_{l+1}x_l)} \tag{25}$$

$$p_{44}^{l}=\frac{m_l\xi_n^{'}(m_{l+1}x_l)\psi_n(m_l x_l)-m_{l+1}\xi_n(m_{l+1}x_l)\psi_n^{'}(m_l x_l)}{m_l\xi_n^{'}(m_{l+1}x_l)\psi_n(m_{l+1}x_l)-m_l\xi_n(m_{l+1}x_l)\psi_n^{'}(m_{l+1}x_l)} \tag{26}$$

Repeat the above process for all interfaces of the multilayered particle, the coefficients of the outmost layer and those of the inner core are linked in the following equations,

$$\begin{bmatrix} a_{mn}^{L+1} \\ b_{mn}^{L+1} \\ c_{mn}^{L+1} \\ d_{mn}^{L+1} \end{bmatrix} = [K]_L \begin{bmatrix} a_{mn}^{1} \\ b_{mn}^{1} \\ c_{mn}^{1} \\ d_{mn}^{1} \end{bmatrix} \tag{27}$$

where the global matrix $[K]_L$ is related to $[P]_L$ as follows,

$$[K]_L=\prod_{l=L}^{1}[P]_l=\begin{bmatrix} k_{11,L} & 0 & 0 & k_{14,L} \\ 0 & k_{22,L} & k_{23,L} & 0 \\ 0 & k_{32,L} & k_{33,L} & 0 \\ k_{41,L} & 0 & 0 & k_{44,L} \end{bmatrix} \tag{28}$$

Note that all necessary information for characterizing the problem is included in one matrix $[K]_l$. As there exists no outgoing field in the inner core, the scattering coefficients a_{mn}^{1} and b_{mn}^{1} are 0. Eliminate c_{mn}^{1} and d_{mn}^{1} from Eq. (27), the following relations are obtained,

$$\begin{bmatrix} a_{mn}^{L+1} \\ b_{mn}^{L+1} \end{bmatrix} = [T] \begin{bmatrix} d_{mn}^{L+1} \\ c_{mn}^{L+1} \end{bmatrix} \tag{29}$$

with

$$\left[T\right]=\begin{bmatrix} T_{11} & 0 \\ 0 & T_{22} \end{bmatrix}=\begin{bmatrix} \dfrac{k_{14,L}}{k_{44,L}} & 0 \\ 0 & \dfrac{k_{23,L}}{k_{33,L}} \end{bmatrix} \tag{30}$$

Eq. (29) represents the relation between the scattering coefficients of a multilayered particle to its incident wave. Note that it recovers to the Mie solution[24] of a solid sphere for L=1.

$$T_{11,solid}=\frac{k_{14,L=1}}{k_{44,L=1}}=\frac{m_2\psi_n^{'}(m_1x_1)\psi_n(m_2x_1)-m_1\psi_n(m_1x_1)\psi_n^{'}(m_2x_1)}{m_1\xi_n^{'}(m_2x_1)\psi_n(m_1x_1)-m_2\xi_n(m_2x_1)\psi_n^{'}(m_1x_1)} \tag{31}$$

$$T_{22,solid}=\frac{k_{23,L=1}}{k_{33,L=1}}=\frac{m_1\psi_n^{'}(m_1x_1)\psi_n(m_2x_1)-m_2\psi_n(m_1x_1)\psi_n^{'}(m_2x_1)}{m_1\xi_n^{'}(m_2x_1)\psi_n(m_2x_1)-m_1\xi_n(m_2x_1)\psi_n^{'}(m_2x_1)} \tag{32}$$

The scattering coefficients of individual particles having been determined, the wave impinging upon a particle, say particle i, in the aggregate is then a sum of the incident wave and the scattered fields from other particles. By the addition theorem, the following relation is obtained,

$$\begin{bmatrix} d_{mn}^{L+1,i} \\ c_{mn}^{L+1,i} \end{bmatrix}=\begin{bmatrix} p_{mn}^{i} \\ q_{mn}^{i} \end{bmatrix}+\begin{bmatrix} \displaystyle\sum_{j=1,j\neq i}^{N}\sum_{n=1}^{N_{\max}}\sum_{m=-n}^{n}A_{mn}^{\mu\nu}(i,j)a_{mn}^{L+1,j} & \displaystyle\sum_{j=1,j\neq i}^{N}\sum_{n=1}^{N_{\max}}\sum_{m=-n}^{n}B_{mn}^{\mu\nu}(i,j)b_{mn}^{L+1,j} \\ \displaystyle\sum_{j=1,j\neq i}^{N}\sum_{n=1}^{N_{\max}}\sum_{m=-n}^{n}B_{mn}^{\mu\nu}(i,j)a_{mn}^{L+1,j} & \displaystyle\sum_{j=1,j\neq i}^{N}\sum_{n=1}^{N_{\max}}\sum_{m=-n}^{n}A_{mn}^{\mu\nu}(i,j)b_{mn}^{L+1,j} \end{bmatrix} \tag{33}$$

where p_{mn}^{i} and q_{mn}^{i} are the coefficients of the incident wave. Here, $A_{mn}^{\mu\nu}(i,j)$ and $B_{mn}^{\mu\nu}(i,j)$ are the vector translation coefficients[49, 50]. Substituting Eq. (33) into Eq. (29), yields the overall scattering coefficients for each specific particle,

$$\begin{aligned}\begin{bmatrix} a_{mn}^{L+1,i} \\ b_{mn}^{L+1,i} \end{bmatrix}&=\begin{bmatrix} T_{11}^{i} & 0 \\ 0 & T_{22}^{i} \end{bmatrix}\begin{bmatrix} p_{mn}^{i} \\ q_{mn}^{i} \end{bmatrix}+\begin{bmatrix} T_{11}^{i} & 0 \\ 0 & T_{22}^{i} \end{bmatrix}\\ &\times\begin{bmatrix} \displaystyle\sum_{j=1,j\neq i}^{N}\sum_{n=1}^{N_{\max}}\sum_{m=-n}^{n}A_{mn}^{\mu\nu}(i,j)a_{mn}^{L+1,j} & \displaystyle\sum_{j=1,j\neq i}^{N}\sum_{n=1}^{N_{\max}}\sum_{m=-n}^{n}B_{mn}^{\mu\nu}(i,j)b_{mn}^{L+1,j} \\ \displaystyle\sum_{j=1,j\neq i}^{N}\sum_{n=1}^{N_{\max}}\sum_{m=-n}^{n}B_{mn}^{\mu\nu}(i,j)a_{mn}^{L+1,j} & \displaystyle\sum_{j=1,j\neq i}^{N}\sum_{n=1}^{N_{\max}}\sum_{m=-n}^{n}A_{mn}^{\mu\nu}(i,j)b_{mn}^{L+1,j} \end{bmatrix}\end{aligned} \tag{34}$$

Let us define

$$\mathbf{g}^{in,i}=\begin{bmatrix} T_{11}^{i} & 0 \\ 0 & T_{22}^{i} \end{bmatrix}\begin{bmatrix} p_{mn}^{i} \\ q_{mn}^{i} \end{bmatrix},\mathbf{G}^{in}=\begin{bmatrix} \mathbf{g}^{in,1} \\ \mathbf{g}^{in,2} \\ \mathbf{g}^{in,3} \\ \vdots \\ \mathbf{g}^{in,N} \end{bmatrix} \tag{35}$$

$$\mathbf{c}^{s,i} = \begin{bmatrix} a_{mn}^{L+1,i} \\ b_{mn}^{L+1,i} \end{bmatrix}, \mathbf{C}^{s} = \begin{bmatrix} \mathbf{c}^{s,1} \\ \mathbf{c}^{s,2} \\ \mathbf{c}^{s,3} \\ \vdots \\ \mathbf{c}^{s,N} \end{bmatrix} \tag{36}$$

$$\mathbf{T}^{j,i} = -\begin{bmatrix} T_{11}^{i} & 0 \\ 0 & T_{22}^{i} \end{bmatrix} \begin{bmatrix} \sum_{j=1, j\neq i}^{N} \sum_{n=1}^{N_{\max}} \sum_{m=-n}^{n} A_{mn}^{\mu\nu}(i,j) a_{mn}^{L+1,j} & \sum_{j=1, j\neq i}^{N} \sum_{n=1}^{N_{\max}} \sum_{m=-n}^{n} B_{mn}^{\mu\nu}(i,j) b_{mn}^{L+1,j} \\ \sum_{j=1, j\neq i}^{N} \sum_{n=1}^{N_{\max}} \sum_{m=-n}^{n} B_{mn}^{\mu\nu}(i,j) a_{mn}^{L+1,j} & \sum_{j=1, j\neq i}^{N} \sum_{n=1}^{N_{\max}} \sum_{m=-n}^{n} A_{mn}^{\mu\nu}(i,j) b_{mn}^{L+1,j} \end{bmatrix} \tag{37}$$

$$\mathbf{T} = \begin{bmatrix} \mathbf{I} & \mathbf{T}^{1,2} & \mathbf{T}^{1,3} & \cdots & \mathbf{T}^{1,N} \\ \mathbf{T}^{2,1} & \mathbf{I} & \mathbf{T}^{2,3} & \cdots & \mathbf{T}^{2,N} \\ \mathbf{T}^{3,1} & \mathbf{T}^{3,2} & \mathbf{I} & \cdots & \mathbf{T}^{3,N} \\ \vdots & \vdots & \vdots & \ddots & \vdots \\ \mathbf{T}^{N,1} & \mathbf{T}^{N,2} & \mathbf{T}^{N,3} & \cdots & \mathbf{I} \end{bmatrix} \tag{38}$$

the system equations for the entire particle aggregates can then be written as

$$\mathbf{T}\mathbf{C}^{s} = \mathbf{G} \tag{39}$$

In practice, the above matrix is solved using the LU decomposition method. Here a different approach is considered, which involves partitioning the above matrix equations into blocks and then applying the elimination procedure to obtain an upper triangular matrix. A natural choice of the blocks for the elimination procedure would be the sub-matrix associated with a particle in the cluster, say, $\mathbf{T}^{1,2}$, though other choices are possible. This is because the unity $\mathbf{I}$ makes calculations easy to start. During the elimination of each column, the sub-matrix terms below the diagonal of the column under consideration and those before it are not changed. For example, during the elimination of the first column, sub-matrices $\mathbf{T}^{2,1}$, …, $\mathbf{T}^{N,1}$ are not changed, though they are used to update other terms. During the elimination of the second column, sub-matrices $\mathbf{T}_{(1)}^{3,2}$ ... $\mathbf{T}_{(2)}^{N,2}$ where the subscript (1) indicates they are updated during the elimination of the first column, and also sub-matrices $\mathbf{T}^{2,1}$, …, $\mathbf{T}^{N,1}$ are unchanged. The procedure proceeds until the last column is considered. This block elimination process results in an updated upper triangular matrix for block back-substitution to obtain the final solution. Since the lower triangular matrix is irrelevant for back-substitution, the terms in the lower triangular matrix that do not require to be updated are not needed in future calculations, and thus are unchanged, thereby resulting in savings in computational time. Because the global matrix is partitioned into sub-matrix blocks, the procedure can be easily implemented in a parallel computing platform, hence leading to further savings in CPU time.

To illustrate the above procedure, let us first define an enhanced matrix, $\mathbf{H}$,

$$\mathbf{H} = \begin{bmatrix} \mathbf{I} & \mathbf{T}^{1,2} & \mathbf{T}^{1,3} & \cdots & \mathbf{T}^{1,N} & \mathbf{g}^{in,1} \\ \mathbf{T}^{2,1} & \mathbf{I} & \mathbf{T}^{2,3} & \cdots & \mathbf{T}^{2,N} & \mathbf{g}^{in,2} \\ \mathbf{T}^{3,1} & \mathbf{T}^{3,2} & \mathbf{I} & \cdots & \mathbf{T}^{3,N} & \mathbf{g}^{in,3} \\ \vdots & \vdots & \vdots & \ddots & \vdots & \vdots \\ \mathbf{T}^{N,1} & \mathbf{T}^{N,2} & \mathbf{T}^{N,3} & \cdots & \mathbf{I} & \mathbf{g}^{in,N} \end{bmatrix} \tag{40}$$

Note that $\mathbf{H}$ contains all the essential information that describes the multiple scattering of the particle cluster.

The block reduction algorithm works as the following procedure:

1. Loop for every row of the entire matrix $\mathbf{H}$. *i* stands for the index of the row number, and it starts from 1 to *N*, where *N* is the number of particles. Repeat the following operations from step 2 to step 4 for each loop *i*.
2. Normalize every block by multiplying the inverse of the diagonal block, which is $\left[\mathbf{H}_{i,i}\right]^{-1}$.
3. Loop for every row below the current row *i*. Let us denote the row index as *j*, which starts from *i*+1 to *N*.
4. Within each row *j*, loop for every block with index as *k*. Note that *k* starts from *i*+1 to *N*. Update each block as

$$\mathbf{H}_{j,k} = \mathbf{H}_{j,i} * \mathbf{H}_{i,k} - \mathbf{H}_{j,k} \tag{41}$$

For instance, with all the operations (from steps 2 to 4) performed for the first loop *i*=1, the matrix $\mathbf{H}$ becomes

$$\mathbf{H}_{(1)} = \begin{bmatrix} \mathbf{I} & \mathbf{T}_{(1)}^{1,2} & \mathbf{T}_{(1)}^{1,3} & \cdots & \mathbf{T}_{(1)}^{1,N} & \mathbf{g}_{(1)}^{in,1} \\ \mathbf{T}^{2,1} & \mathbf{I} & \mathbf{T}_{(1)}^{2,3} & \cdots & \mathbf{T}_{(1)}^{2,N} & \mathbf{g}_{(1)}^{in,2} \\ \mathbf{T}^{3,1} & \mathbf{T}_{(1)}^{3,2} & \mathbf{I} & \cdots & \mathbf{T}_{(1)}^{3,N} & \mathbf{g}_{(1)}^{in,3} \\ \vdots & \vdots & \vdots & \ddots & \vdots & \vdots \\ \mathbf{T}^{N,1} & \mathbf{T}_{(1)}^{N,2} & \mathbf{T}_{(1)}^{N,3} & \cdots & \mathbf{I} & \mathbf{g}_{(1)}^{in,N} \end{bmatrix} \tag{42}$$

With all the above procedures completed, the entire matrix $\mathbf{H}$ is updated as

$$\mathbf{H}_{updated} = \begin{bmatrix} \mathbf{I} & \mathbf{T}_{(1)}^{1,2} & \mathbf{T}_{(1)}^{1,3} & \cdots & \mathbf{T}_{(1)}^{1,N} & \mathbf{g}_{(1)}^{in,1} \\ \mathbf{T}^{2,1} & \mathbf{I} & \mathbf{T}_{(2)}^{2,3} & \cdots & \mathbf{T}_{(2)}^{2,N} & \mathbf{g}_{(2)}^{in,2} \\ \mathbf{T}^{3,1} & \mathbf{T}_{(1)}^{3,2} & \mathbf{I} & \cdots & \mathbf{T}_{(3)}^{3,N} & \mathbf{g}_{(3)}^{in,3} \\ \vdots & \vdots & \vdots & \ddots & \vdots & \vdots \\ \mathbf{T}^{N,1} & \mathbf{T}_{(1)}^{N,2} & \mathbf{T}_{(2)}^{N,3} & \cdots & \mathbf{I} & \mathbf{g}_{(N)}^{in,N} \end{bmatrix} \tag{43}$$

5. Substituting backward from the bottom row to the top. Let us denote the row index as *l*, which starts from *N* to 1.
6. Within each loop *l*, the block matrix $\mathbf{c}^{s,l}$ that contains the scattering coefficients of particle *l* is calculated as

$$\mathbf{c}^{s,l} = \mathbf{g}_l^{in,l} - \sum_{l=N}^{1} \sum_{m=N}^{l+1} \mathbf{T}_l^{l,m} \mathbf{c}^{s,m} \tag{44}$$

In the results obtained below, the above algorithm is slightly modified such that the global matrix is not formed, and instead the submatrix is created. In this way, the calculations are performed as soon as submatrix blocks are available. This will not only save the storage space but also some computing time in forming global and then submatrices. To illustrate the concept of the algorithm, however, the description with reference to the global matrix is much easier to understand.

With all the scattering coefficients of individual particles determined, the effective scattering efficiency of the entire particle aggregates is expressed as[51]

$$Q_{sca}=\frac{4}{(kr)^2}\sum_{n=1}^{N_{\max}}\sum_{m=-n}^{n}\sum_{j=1}^{NT}\Bigg(\left(a_{mn}^{L+1,j}a_{mn}^{*L+1,j}+b_{mn}^{L+1,j}b_{mn}^{*L+1,j}\right)\frac{n(n+1)(n+m)!}{(2n+1)(n-m)!}$$

$$+2\,\mathrm{Re}\sum_{\nu=1}^{N_{\max}}\sum_{\mu=-\nu}^{\nu}\sum_{\lambda>j}^{NT}\Big[\left(a_{mn}^{L+1,j}a_{\mu\nu}^{*L+1,\lambda}+b_{mn}^{L+1,j}b_{\mu\nu}^{*L+1,\lambda}\right)C_{mn}^{\mu\nu}(i,j) \tag{45}$$

$$+\left(b_{mn}^{L+1,j}a_{\mu\nu}^{*L+1,\lambda}+a_{mn}^{L+1,j}b_{\mu\nu}^{*L+1,\lambda}\right)D_{mn}^{\mu\nu}(i,j)\Big]\Bigg)$$

with

$$C_{mn}^{\mu\nu}(i,j)=\frac{(-1)^{\mu+n}}{2}\frac{(n+m)!}{(n-m)!}\sum_{p=|n-\nu|}^{n+\nu}i^{p+n+\nu}c_{mn}^{\mu\nu}(p)\,j_p(ku_{\lambda l})P_p^{m-\mu}(\cos\theta_{\lambda l})e^{i(m-\mu)\varphi_{\lambda l}} \tag{46}$$

$$D_{mn}^{\mu\nu}(i,j)=(-1)^{\mu+1}\sum_{p=|n-\nu|}^{n+\nu}i^{p-n+\nu}\frac{1-(-1)^{p+\nu+n}}{2}(2p+1)$$

$$\times\begin{pmatrix}p & n & \nu\\ 0 & 1 & -1\end{pmatrix}\begin{pmatrix}p & n & \nu\\ -m+\mu & m & -\mu\end{pmatrix}\sqrt{\frac{(n+m)!(\nu+\mu)!(p-m+\mu)!}{(n-m)!(\nu-\mu)!(p+m-\mu)!}} \tag{47}$$

$$\times j_p(ku_{\lambda l})P_p^{m-\mu}(\cos\theta_{\lambda l})e^{i(m-\mu)\varphi_{\lambda l}}$$

$$c_{mn}^{\mu\nu}(p)=\left[n(n+1)+\nu(\nu+1)-p(p+1)\right]\frac{(p-m+\mu)!}{(p+m-\mu)!}a_{-mn}^{\mu\nu}(p) \tag{48}$$

$$a_{mn}^{\mu\nu}(p)=(-1)^{-\mu-m}(2p+1)\sqrt{\frac{(n+m)!(\nu+\mu)!(p-m-\mu)!}{(n-m)!(\nu-\mu)!(p+m+\mu)!}} \tag{49}$$

$$\times\begin{pmatrix}n & \nu & p\\ 0 & 0 & 0\end{pmatrix}\begin{pmatrix}n & \nu & p\\ m & \mu & -m-\mu\end{pmatrix}$$

3. Results and discussions

To verify the computational efficiency of the above algorithm, the computational time consumed to solve the system equations for various numbers of particles is evaluated by both the LU decomposition method and the proposed block elimination approach. In the calculation, each block has the size of $2\times N_{\max}$ by $2\times N_{\max}$, with $N_{\max}$ being the number of unknown scattering coefficients (*a* or *b*) of each particle. Clusters containing various numbers of identical nanoshells are selected for testing at 400 nm wavelength. Each nanoparticle has Si/Ag/Si three-layered structure, with radii of 40 nm, 60 nm, and 90 nm, respectively. $N_{\max}$ is set as 6 since the contributions of higher modes are negligible. The run time of the block elimination algorithm presented is compared with that of LU decomposition method in Fig. 2. As shown in the result, the block elimination method saves ~7-10% in comparison with the LU decomposition method. For multiple scattering problems that contain many particle particles, calculations for a scattering curve over a range of spectrums may take hours to complete, for which case the present method is a considerable enhancement of the computation efficiency. We attribute CPU improvement to two aspects. First, the proposed approach performs eliminations only for blocks that have higher column indices than that of the pivot block. That is, there are not any operations on the blocks with lower column indices than that of the pivot block. Second, during the normalization process for each row, the diagonal block is only inversed once. The inversed block is kept and shared throughout the elimination operations for all the remaining blocks in the same row. As discussed above, the block elimination computational procedure can be readily parallelized. Tests show that a drastic reduction in CPU

time (up to 40% reduction) is obtained, when the block elimination is implemented within the framework of parallel computing, as illustrated in Fig. 2. It is further noticed that for the present case, the reduction in CPU is much more significant for the number of particles up to 25 and gradually levels off as the number of the particles increases.

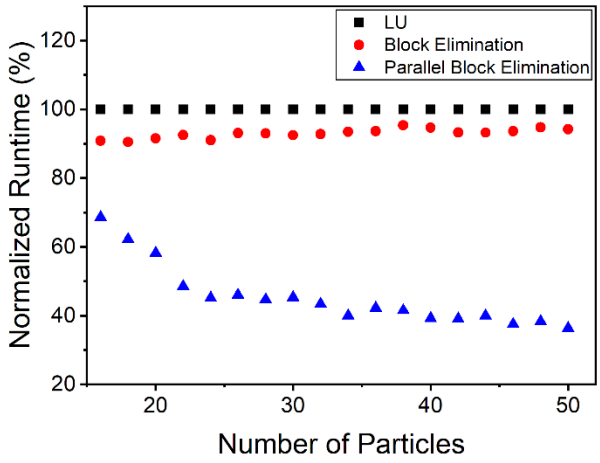

Fig. 2. Computation time of LU decomposition method, the block elimination approach, and the parallel block elimination method.

With the computational efficiency validated, the presented methodology can be applied to explore various light-scattering responses of multilayered nanoparticle aggregates. In this part, several nanoparticle arrangements are investigated. They are two-dimensional nanoparticle rings, three-dimensional nanoshell clusters, nanoshell mixtures, and large dielectric spheres decorated with orderly-arranged metal particles.

Fig. 3(a) plots the scattering efficiency of a nanoparticle ring located in the **E-H** plane, which is perpendicular to the wave propagation direction. The overall effective scattering efficiency of the particle ring configuration is denoted as total, while the electric dipole, electric quadrupole, magnetic dipole, and magnetic quadrupole mode contributions are denoted as a_1, a_2, b_1, and b_2, respectively. The nanoparticle ring consists of six identical nanoshells with Si/Ag/Si three-layered structure. Each nanoshell has 40 nm, 60 nm, and 90 nm radii for inner silicon, intermedium silver, and outer silicon layers, respectively. The gap between every particle is set to 10 nm. As shown in Fig. 3(a), both peaks of the effective electric and magnetic dipoles are tuned to 600 nm. That is, it satisfies the maximum forward scattering condition[52], which requires both the electric and magnetic dipole modes to oscillate in phase and have relatively comparable magnitudes. Fig. 3(b) shows the corresponding forward scattering efficiency (denoted as Q_f), backward scattering efficiency (denoted as Q_b), and scattering efficiency along the direction perpendicular to the wave propagation efficiency (denoted as Q_{side}), appended with the scattering patterns at distinct wavelength peaks. As shown in the result, a maximum forward scattering peak appears around 600 nm. Moreover, the nanoparticle ring shows a broadband forward scattering response between 420 nm and 575 nm. Several forward scattering peaks are observed at 460 nm, 495 nm, and 540 nm, where the directional scattering behaviors originated from the hybridization of the electric dipole, magnetic dipole, and magnetic quadrupole modes.

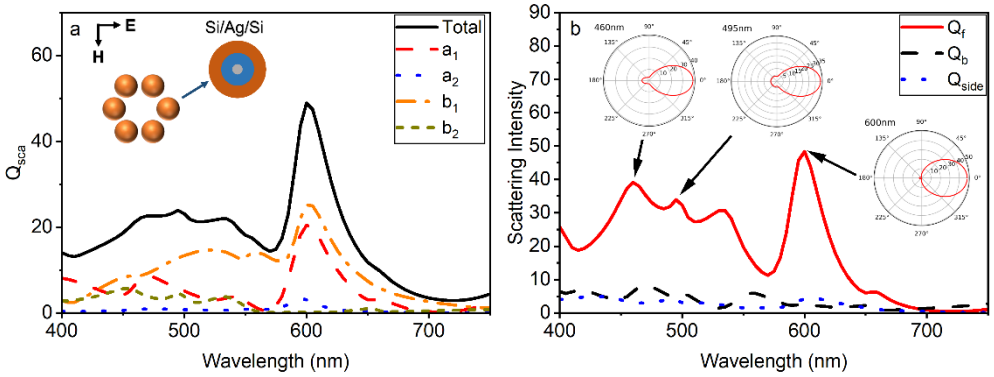

Fig. 3. (a) Scattering efficiency with its electric and magnetic modes contributions of a nanoring structure containing six Si/Ag/Si three-layered rattling nanoshells. (b) Forward scattering efficiency, backward scattering efficiency, and scattering efficiency along the direction perpendicular to the wave propagation. Scattering patterns at distinct peaks are displayed.

With the 2-D nanoparticle configuration studied, let us consider a 3-D case where a SiO_2/Si nanoshell is surrounded by six SiO_2/Ag nanoshells. The six outer particles are displaced in the +**k**, -**k**, +**E**, -**E**, +**H**, and -**H** axis, respectively. All particles have identical radii of the layers as 70 nm and 90 nm for the core and shell, respectively. The gap between the center particle and every surrounding one is 10 nm. As displayed in Fig. 4(a), the dominating mode is the effective magnetic dipole and the effective magnetic quadruple mode located at 575 nm and 505 nm, respectively. The electric dipole possesses a relatively flatter peak of around 720 nm. Such peak features may be explained as follows. For the 3-D nanoparticle structure, both the center and surrounding nanoshells possess electric dipole modes. The difference is that the dipole of the center particle mainly originated from the silicon shell, while the ones of the surrounding particles are from the silver shell. In other words, the distinction in materials results in electric dipoles with distinct peak wavelengths and magnitudes. As a result, the interactions between those modes form flat effective electric dipole peaks. The magnetic dipole modes mainly exist in the center nanoparticle, which contains high refractive index silicon. Therefore, the effective magnetic dipole and quadruple modes have relatively sharp peaks. The examination of resultant directional scattering intensity, displayed in Fig 4. (b), shows a dominating side scattering peak at 505 nm, a wide-angle forward scattering feature at 575 nm, and a backward scattering response at 720 nm. It is further confirmed by the scattering patterns shown in Fig. 4(b). It is worth noting that the particle aggregates show opposite scattering directionalities at those adjacent wavelengths, which may be applicable to the realization of the optical switch.

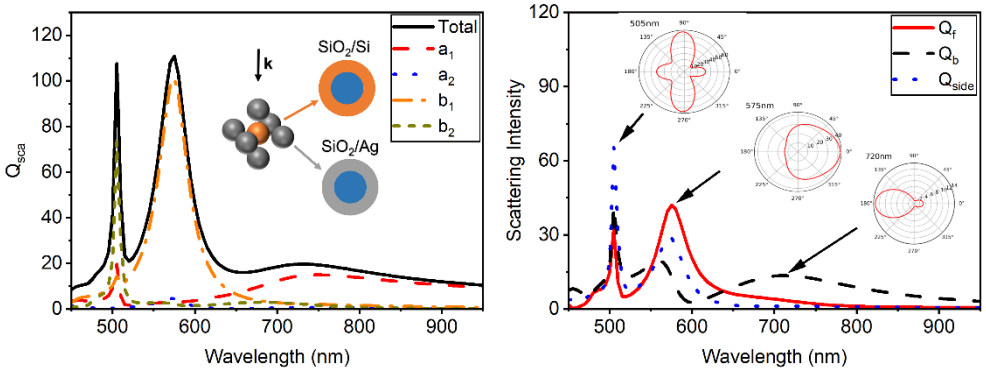

Fig. 4. (a) Scattering efficiency with its electric and magnetic modes contributions of a cluster of seven nanoshells. (b) Forward scattering efficiency, backward scattering efficiency, and scattering efficiency along the direction perpendicular to the wave propagation.

Another type of multi-nanoparticle arrangement is an aggregate of mixed nanoshells with distinct materials and structures. Fig. 5(a) presents the scattering efficiency of a nanoshell aggregate consisting of eight particles. It contains two types of nanostructures, i.e., the Air/SiO_2/Si and the Air/SiO_2/Ag three-layered nanoshells. The radii of layers for each Air/SiO_2/Si particle are 40 nm, 65 nm, and 90 nm, while those for each Air/SiO_2/Ag particle are 20 nm, 50 nm, and 90 nm, respectively. The gap between every particle is 10 nm. The results illustrate that the effective electric dipole, magnetic dipole, and magnetic quadrupole modes are tuned to 610 nm, resulting in a sharp forward scattering intensity peak as shown in Fig. 5(b). Such a sharp strong forward scattering peak is due to the in-phase oscillation of those diverse modes.

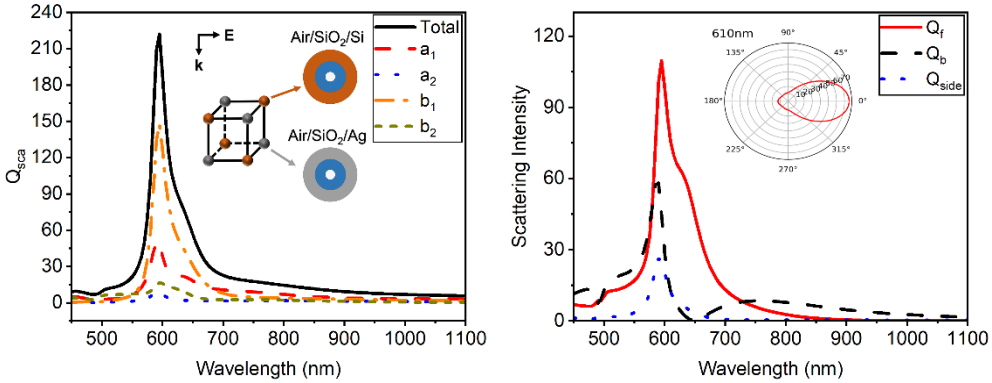

Fig. 5. (a) Scattering efficiency with its electric and magnetic modes contributions of a 3D mixed structure containing eight nanoshells. (b) Forward scattering efficiency, backward scattering efficiency, and scattering efficiency along the direction perpendicular to the wave propagation.

A more complex nanoshell aggregate mixture is considered further. Fig. 6(a) displays the scattering efficiency of a nanoshell aggregate consisting of twenty-seven particles, where a large TiO_2 nanosphere is decorated with twenty-six orderly-arranged Ag nanoparticles. Several forward scattering peaks are observed in Fig. 6(b) at 520 nm, 580 nm, and 820 nm, respectively. They are the result of the complex hybridization of the effective electric and magnetic dipole and quadrupole modes that comes from the interactions of the decorating Ag particles and the TiO_2 core.

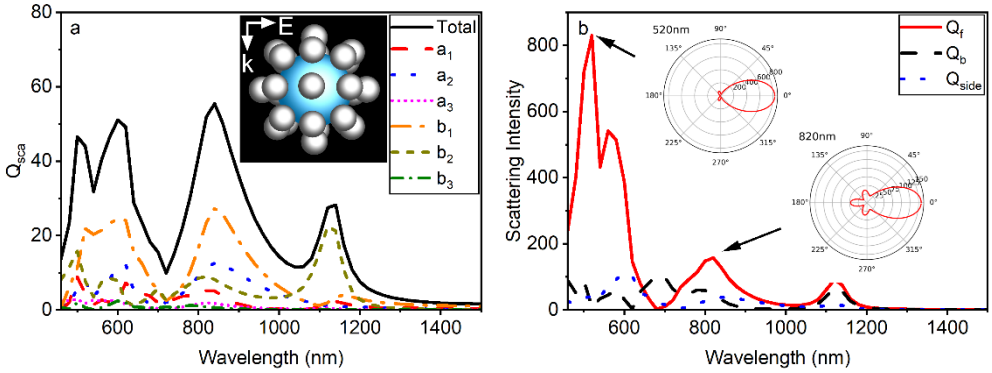

Fig. 6. (a) Scattering efficiency with its electric and magnetic modes contributions of a hybrid nanostructure of a large TiO_2 nanosphere decorated with orderly-arranged Ag nanoparticles. (b) Forward scattering efficiency, backward scattering efficiency, and scattering efficiency along the direction perpendicular to the wave propagation.

4. Conclusion

This paper has presented an efficient computational method for the solution of the multiple scattering problem of multilayered nanoshell aggregates. The approach entails dividing global matrix for multiple particles into submatrices (or blocks) and updating only partial blocks of individual rows in every iteration. In addition, the algorithm saves the calculation load with the pivot block inversed once for every single row. The present block elimination procedure can be easily implemented within the framework of parallel computing. A selection of results is presented. Numerical tests show that a significant reduction in CPU time can be obtained with the parallelized block elimination procedure. Illustrative cases studied show various optical responses, including broadband forward scattering, strong forward scattering with sharp peaks, and strong backward scattering features that can be achieved with specific particle arrangements.

Acknowledgments. Partial of this work is supported by the M-Cube program and Sunshine Energy Inc (Grant #: N028639).

Disclosures. The authors declare that there are no conflicts of interest related to this article.

Data availability. Data underlying the results presented in this paper are not publicly available at this time but may be obtained from the authors upon reasonable request.

References

1. Kumar A, Choudhary P, Kumar A, et al (2022) Recent Advances in Plasmonic Photocatalysis Based on TiO_2 and Noble Metal Nanoparticles for Energy Conversion, Environmental Remediation, and Organic Synthesis. Small 18:2101638. https://doi.org/10.1002/smll.202101638

2. Zhu Q, Xuan Y, Zhang K, Chang K (2021) Enhancing photocatalytic CO_2 reduction performance of g-C_3N_4-based catalysts with non-noble plasmonic nanoparticles. Applied Catalysis B: Environmental 297:120440. https://doi.org/10.1016/j.apcatb.2021.120440

3. Ren H, Yang J-L, Yang W-M, et al (2021) Core–Shell–Satellite Plasmonic Photocatalyst for Broad-Spectrum Photocatalytic Water Splitting. ACS Materials Lett 3:69–76. https://doi.org/10.1021/acsmaterialslett.0c00479

4. Abouelela MM, Kawamura G, Matsuda A (2021) A review on plasmonic nanoparticle-semiconductor photocatalysts for water splitting. Journal of Cleaner Production 294:126200. https://doi.org/10.1016/j.jclepro.2021.126200

5. Abed J, Rajput NS, Moutaouakil AE, Jouiad M (2020) Recent Advances in the Design of Plasmonic Au/TiO_2 Nanostructures for Enhanced Photocatalytic Water Splitting. Nanomaterials 10:2260. https://doi.org/10.3390/nano10112260

6. Venkatachalam P, Kalaivani T, Krishnakumar N (2019) Erbium doped anatase TiO_2 nanoparticles for photovoltaic applications. Opt Quant Electron 51:315. https://doi.org/10.1007/s11082-019-2034-2

7. Balakrishnan M, John R (2021) Impact of Ni metal ion concentration in TiO_2 nanoparticles for enhanced photovoltaic performance of dye sensitized

solar Cell. J Mater Sci: Mater Electron 32:5295–5308. https://doi.org/10.1007/s10854-020-05100-0

8. Daneshfar N (2021) The Study of Scattering-to-absorption Ratio in Plasmonic Nanoparticles for Photovoltaic Cells and Sensor Applications. Plasmonics 16:2017–2023. https://doi.org/10.1007/s11468-021-01464-z

9. Chaudhry FA, Escandell L, López-Fraguas E, et al (2022) Light absorption enhancement in thin film GaAs solar cells using dielectric nanoparticles. Sci Rep 12:9240. https://doi.org/10.1038/s41598-022-13418-4

10. Rezaeian A, Amini SM, Najafabadi MRH, et al (2022) Plasmonic hyperthermia or radiofrequency electric field hyperthermia of cancerous cells through green-synthesized curcumin-coated gold nanoparticles. Lasers Med Sci 37:1333–1341. https://doi.org/10.1007/s10103-021-03399-7

11. de la Encarnación C, Jimenez de Aberasturi D, Liz-Marzán LM (2022) Multifunctional plasmonic-magnetic nanoparticles for bioimaging and hyperthermia. Advanced Drug Delivery Reviews 189:114484. https://doi.org/10.1016/j.addr.2022.114484

12. Bucharskaya AB, Khlebtsov NG, Khlebtsov BN, et al (2022) Photothermal and Photodynamic Therapy of Tumors with Plasmonic Nanoparticles: Challenges and Prospects. Materials 15:1606. https://doi.org/10.3390/ma15041606

13. Xing M, Mohapatra J, Beatty J, et al (2021) Iron-based magnetic nanoparticles for multimodal hyperthermia heating. Journal of Alloys and Compounds 871:159475. https://doi.org/10.1016/j.jallcom.2021.159475

14. D'Acunto M, Cioni P, Gabellieri E, Presciuttini G (2021) Exploiting gold nanoparticles for diagnosis and cancer treatments. Nanotechnology 32:192001. https://doi.org/10.1088/1361-6528/abe1ed

15. Ziai Y, Rinoldi C, Nakielski P, et al (2022) Smart plasmonic hydrogels based on gold and silver nanoparticles for biosensing application. Current Opinion in Biomedical Engineering 24:100413. https://doi.org/10.1016/j.cobme.2022.100413

16. Staniszewska T, Szkulmowski M, Morawiec S (2021) Computational Optimization of the Size of Gold Nanorods for Single-Molecule Plasmonic Biosensors Operating in Scattering and Absorption Modes. J Phys Chem C 125:14765–14777. https://doi.org/10.1021/acs.jpcc.1c02510

17. Ou X, Liu Y, Zhang M, et al (2021) Plasmonic gold nanostructures for biosensing and bioimaging. Microchim Acta 188:304. https://doi.org/10.1007/s00604-021-04964-1

18. Hassan MM, Sium FS, Islam F, Choudhury SM (2021) A review on plasmonic and metamaterial based biosensing platforms for virus detection. Sensing and Bio-Sensing Research 33:100429. https://doi.org/10.1016/j.sbsr.2021.100429

19. Altenschmidt L, Sánchez-Paradinas S, Lübkemann F, et al (2021) Aerogelation of Polymer-Coated Photoluminescent, Plasmonic, and Magnetic Nanoparticles for Biosensing Applications. ACS Appl Nano Mater 4:6678–6688. https://doi.org/10.1021/acsanm.1c00636

20. Fuertes V, Grégoire N, Labranche P, et al (2021) Engineering nanoparticle features to tune Rayleigh scattering in nanoparticles-doped optical fibers. Sci Rep 11:9116. https://doi.org/10.1038/s41598-021-88572-2

21. Zhang X, Yang J (2019) Ultrafast Plasmonic Optical Switching Structures and Devices. Frontiers in Physics 7:

22. Jiang L, Yin T, Dubrovkin AM, et al (2019) In-plane coherent control of plasmon resonances for plasmonic switching and encoding. Light Sci Appl 8:21. https://doi.org/10.1038/s41377-019-0134-1

23. Li Y, Shao L, Zhong F, et al (2018) Light control based on unidirectional scattering in metal–dielectric core–shell nanoparticles. Optics Communications 426:483–489. https://doi.org/10.1016/j.optcom.2018.05.075

24. Bohren CF, Huffman DR (1983) Absorption and scattering of light by small particles. Wiley, New York

25. Diress Gesesse G, Neel TL, Cui Z, et al (2018) Plasmonic core–shell nanostructure as an optical photoactive nanolens for enhanced light harvesting and hydrogen production. Nanoscale 10:20140–20146. https://doi.org/10.1039/C8NR07475E

26. Ge L, Liu L, Dai S, et al (2017) Unidirectional scattering induced by the toroidal dipolar excitation in the system of plasmonic nanoparticles. Opt Express, OE 25:10853–10862. https://doi.org/10.1364/OE.25.010853

27. Manai L, Dridi Rezgui B, Benabderrahmane Zaghouani R, et al (2016) Tuning of Light Trapping and Surface Plasmon Resonance in Silver Nanoparticles/c-Si Structures for Solar Cells. Plasmonics 11:1273–1277. https://doi.org/10.1007/s11468-015-0171-4

28. Li Y, Wan M, Wu W, et al (2015) Broadband zero-backward and near-zero-forward scattering by metallo-dielectric core-shell nanoparticles. Sci Rep 5:12491. https://doi.org/10.1038/srep12491

29. Liu W, Zhang J, Lei B, et al (2014) Ultra-directional forward scattering by individual core-shell nanoparticles. Opt Express 22:16178. https://doi.org/10.1364/OE.22.016178

30. Liu W, Miroshnichenko AE, Neshev DN, Kivshar YS (2012) Broadband Unidirectional Scattering by Magneto-Electric Core–Shell Nanoparticles. ACS Nano 6:5489–5497. https://doi.org/10.1021/nn301398a

31. Sun S, Wang D, Feng Z, Tan W (2020) Highly efficient unidirectional forward scattering induced by resonant interference in a metal–dielectric heterodimer. Nanoscale 12:22289–22297. https://doi.org/10.1039/D0NR07010F

32. Yang W (2003) Improved recursive algorithm for light scattering by a multilayered sphere. Appl Opt, AO 42:1710–1720. https://doi.org/10.1364/AO.42.001710

33. Sinzig J, Quinten M (1994) Scattering and absorption by spherical multilayer particles. Appl Phys A 58:157–162. https://doi.org/10.1007/BF00332172

34. Mackowski DW, Mishchenko MI (1996) Calculation of the T matrix and the scattering matrix for ensembles of spheres. J Opt Soc Am A, JOSAA 13:2266–2278. https://doi.org/10.1364/JOSAA.13.002266

35. Mackowski DW (1991) Analysis of radiative scattering for multiple sphere configurations. Proceedings of the Royal Society of London Series A: Mathematical and Physical Sciences 433:599–614. https://doi.org/10.1098/rspa.1991.0066

36. Xu Y (1995) Electromagnetic scattering by an aggregate of spheres. Appl Opt, AO 34:4573–4588. https://doi.org/10.1364/AO.34.004573

37. Mackowski DW (2014) A general superposition solution for electromagnetic scattering by multiple spherical domains of optically active media. Journal of Quantitative Spectroscopy and Radiative Transfer 133:264–270. https://doi.org/10.1016/j.jqsrt.2013.08.012

38. Liu C, Li BQ (2011) Computational Multiscattering of Spherical Multilayered Gold Nanoshells. J Phys Chem C 115:5323–5333. https://doi.org/10.1021/jp110252r

39. Li BQ, Liu C (2012) Multi-scattering of electromagnetic waves by nanoshell aggregates. J Nanopart Res 14:839. https://doi.org/10.1007/s11051-012-0839-z

40. Egel A, Czajkowski KM, Theobald D, et al (2021) SMUTHI: A python package for the simulation of light scattering by multiple particles near or between planar

interfaces. Journal of Quantitative Spectroscopy and Radiative Transfer 273:107846. https://doi.org/10.1016/j.jqsrt.2021.107846

41. Stout B, Auger J-C, Lafait J (2002) A transfer matrix approach to local field calculations in multiple-scattering problems. Journal of Modern Optics 49:2129–2152. https://doi.org/10.1080/09500340210124450

42. Stout B, Auger JC, Devilez A (2008) Recursive T matrix algorithm for resonant multiple scattering: applications to localized plasmon excitations. J Opt Soc Am A, JOSAA 25:2549–2557. https://doi.org/10.1364/JOSAA.25.002549

43. Mackowski DW (1994) Calculation of total cross sections of multiple-sphere clusters. J Opt Soc Am A, JOSAA 11:2851–2861. https://doi.org/10.1364/JOSAA.11.002851

44. Egel A, Pattelli L, Mazzamuto G, et al (2017) CELES: CUDA-accelerated simulation of electromagnetic scattering by large ensembles of spheres. Journal of Quantitative Spectroscopy and Radiative Transfer 199:103–110. https://doi.org/10.1016/j.jqsrt.2017.05.010

45. Markkanen J, Yuffa AJ (2017) Fast superposition T-matrix solution for clusters with arbitrarily-shaped constituent particles. Journal of Quantitative Spectroscopy and Radiative Transfer 189:181–188. https://doi.org/10.1016/j.jqsrt.2016.11.004

46. Törmä MNP (2021) Multiple-Scattering T-Matrix Simulations for Nanophotonics: Symmetries and Periodic Lattices. CiCP 30:357–395. https://doi.org/10.4208/cicp.OA-2020-0136

47. Schebarchov D, Fazel-Najafabadi A, Le Ru EC, Auguié B (2022) Multiple scattering of light in nanoparticle assemblies: User guide for the terms program. Journal of Quantitative Spectroscopy and Radiative Transfer 284:108131. https://doi.org/10.1016/j.jqsrt.2022.108131

48. Aden AL, Kerker M (1951) Scattering of Electromagnetic Waves from Two Concentric Spheres. Journal of Applied Physics 22:1242–1246. https://doi.org/10.1063/1.1699834

49. Stein S (1961) Addition theorems for spherical wave functions. Quart Appl Math 19:15–24. https://doi.org/10.1090/qam/120407

50. Cruzan OR (1962) Translational Addition Theorems for Spherical Vector Wave Functions. Quarterly of Applied Mathematics 20:33–40

51. Liu CH, Li BQ (2013) Energy Absorption in Gold Nanoshells. Journal of Nano Research 23:74–82. https://doi.org/10.4028/www.scientific.net/JNanoR.23.74

517 52. Kerker M, Wang D-S, Giles CL (1983) Electromagnetic scattering by magnetic
518 spheres. J Opt Soc Am 73:765. https://doi.org/10.1364/JOSA.73.000765

519